STRUCTURE AND ELECTROCHEMICAL IMPEDANCE OF LiNi$_x$Mn$_{2-x}$O$_4$

TA ANH TAN[1,4], NGUYEN SI HIEU[1], LE HA CHI[1], DANG TRAN CHIEN[2]
LE DINH TRONG[3] AND PHAM DUY LONG[1,†]

[1]*Institute of Materials Science, Vietnam Academy of Science and Technology,*
18-Hoang Quoc Viet, Cau Giay, Hanoi, Vietnam

[2]*Hanoi University of Natural Resources and Environment,*
41A-Phu Dien, Bac Tu Liem, Hanoi, Vietnam

[3]*Hanoi Pedagogical University No. 2,*
32-Nguyen Van Linh, Xuan Hoa, Phuc Yen, Vinh Phuc, Vietnam

[4]*Hanoi Metropolitan University, 98-Duong Quang Ham, Cau Giay, Hanoi, Vietnam*

[†]*E-mail:* longphd@ims.vast.ac.vn

Abstract. *Ni-substitution spinel LiNi$_x$Mn$_{2-x}$O$_4$ $(x = 0, 0.1, 0.2)$ materials were synthesized by the sol–gel method. The structure and morphology of the samples were characterized by the X-ray diffraction (XRD) and the scanning electron microscopy. The ac conduction of the materials was investigated by electrochemical impedance spectroscopy (EIS) measurements. The refinement results showed that the substitution of Ni decreased the lattice constant and Mn–O distance, while increased Li–O bond length and 16c octahedral volume. The EIS results confirmed the decrease of conductivity with increasing Ni substitution content. Based on XRD and EIS results, the relationship between the crystal structure and electrochemical behavior of the materials was discussed and explained.*

Keywords: lithium ion battery, spinel manganate cathode material, Rietveld refinement, Electrochemical impedance.

Classification numbers: 82.47.Aa, 61.05.cp, 61.72.-y.

I. INTRODUCTION

The efforts for the development of energy storage systems have been forced rapidly due to the increase in the demand of clean and renewable energy sources. Lithium ion batteries have been considered as the most attractive energy storage system due to its advantages including high energy density and long cycle life. However, the issues of cost, safety and capacity of conventional

cathode materials such as $LiCoO_2$ required the development of new cathode materials. Recently, $LiMn_2O_4$ spinel cathode materials attracted a lot of interest due to its low cost, environmental friendliness and safety [1, 2]. However, this cathode material faced some problems including Mn dissolution in electrolytes [3], Jahn-Teller distortion at deeply discharge [4], and oxygen deficiency [5]. The substitution of Mn by other elements such as Ni, Al, Fe, Co resulted in the improvement in the electrochemical performance of the mother material [6]. Excellent electrochemical performance of $LiNi_{0.5}Mn_{1.5}O_4$ cathode material has confirmed by many group [7, 8]. Nevertheless, this material is quite expensive due to the high amount of nickel. In this circumstance, the studies of $LiNi_xMn_{2-x}O_4$ at low substitution levels are very necessary.

It is recognised that the electrochemical properties of manganate spinels depend on the preparation method [9–11]. In addition, published studies showed controversial results about the effect of Ni substitution on the conductivity of $LiNi_xMn_{2-x}O_4$. For example, while J. Molenda *et al.* [12] showed the decrease of the conductivity by Ni substitution, M. A. Kebede *et al.* [13] announced opposite results. Especially, there has not been adequate attention paid to studying the effect of structure on the conductivity of $LiNi_xMn_{2-x}O_4$ materials. In this work, $LiNi_xMn_{2-x}O_4$ $(x = 0, 0.1, 0.2)$ was synthesized by the sol-gel method. The effect of Ni substitution level on the structure of the material was investigated. Based on the experiment results, the relationship between the structure and the conductivity of the material was discussed. In addition, the study of structure also contributed to explain the effect of Ni substitution on the electrochemical performance of $LiNi_xMn_{2-x}O_4$ cathode materials

II. EXPERIMENTAL

$LiMn_{2-x}Ni_xO_4$ $(x = 0, 0.1, 0.2)$ materials have synthesized by the sol-gel method. The stoichiometric amounts of analytical grade of lithium acetate ($CH_3COOLi.2H_2O$), manganese II acetate ($2(CH_3COO)Mn.4H_2O$) and nickel II acetate ($2(CH_3COO)Ni.4H_2O$) from Sigma Aldrich were separately dissolved in deionized distilled water followed by the continuous stirring at 80˚C. The mixtures were stirred for 1h to form a clear homogeneous solution. The solutions then were added by citric acid ($CH_2COOH–C(OH)COOH–CH_2COOH$, Sigma Aldrich, 99.9%) with a molar ratio of 1 lithium acetate: 3 citric acid followed by the continuous stirring for 8 h. The final solutions were dried at 120˚C for 12 h and then calcined in air at 800˚C for 15h to obtain the materials.

The SEM images of the materials were obtained by using Hitachi S-4800 FESEM. The X-ray powder diffraction analyses of the materials were performed by Siemens D5000 X-ray diffractometer using $CuK\alpha$ radiation at room temperature. The filament bias voltage and the filament current were set at 35 kV and 40 mA respectively. The angle of diffraction (2θ) was changed from 10˚ to 70˚ at a step of 0.03˚/sec. The Rietveld refinement of X-ray diffraction data was conducted by the FullProf software package [14]. The crystal structures were drawn by VESTA programs [15].

For the measurements of electrochemical impedance, the powders were uniaxially cold pressed at 40 MPa to form cylindrical pellets with the diameter of ca. 12 mm and the thickness of ca. 1.5 mm. The electrodes were prepared by the evaporation of Au on the pellets. The diameter and the thickness of the electrodes were ca. 8mm and 1μm, respectively. The impedance measurements were carried out by EIS-Zahner IM 6 electrochemical impedance analyzer at amplitude of

10 mV and frequency range of 10^{-1}–10^6 Hz. The fitting of EIS data was performed by the Zview software.
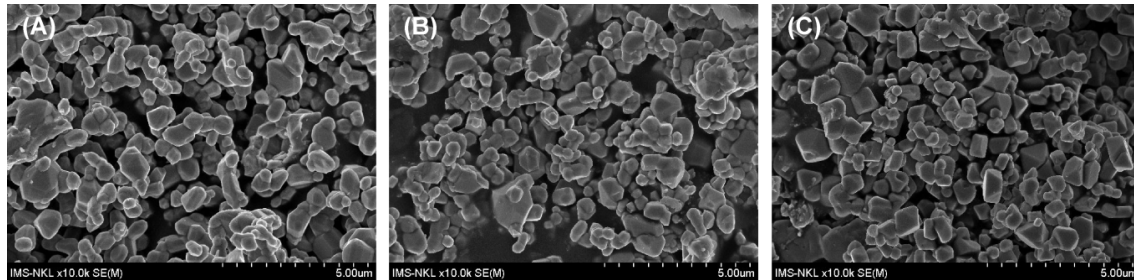
III. RESULTS AND DISCUSSION

Fig. 1. SEM images of the $LiMn_2O_4$ (a), $LiMn_{1.9}Ni_{0.1}O_4$ (b) and $LiMn_{1.8}Ni_{0.2}O_4$ (c) powders (a, b, c) that were calcined at 800°C.

The SEM observations of the $LiMn_{2-x}Ni_xO_4$ ($x = 0, 0.1, 0.2$) powders were showed in Fig. 1. Generally, the particle size of the un-doped and doped samples was quite similar. The particle sizes of the samples were in the range of 300 nm – 1μm. It is easy to see that the shape of the particles changed from round to sharp with increasing substitution content. This fact showed that Ni substitution affected on the morphology of the crystalline-particle shape.
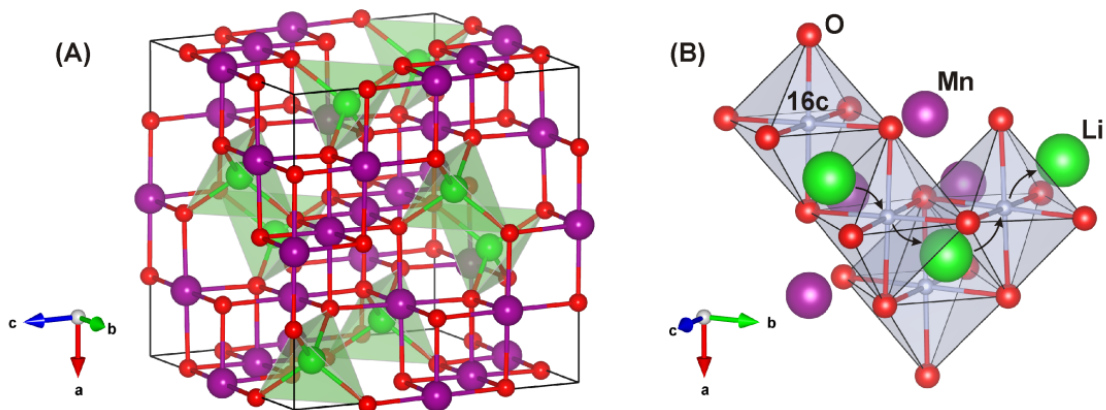

Fig. 2. The crystal structure of $LiMn_2O_4$ material (a). And the illustration of Li^+ diffusion via 16c site (b). Black arrows showed the diffusion pathway of Li^+ ion.

The structure of the materials was investigated by XRD measurements. Rietveld refinement was used to refine the patterns. At room temperature, $LiMn_2O_4$ has cubic-spinel structure with the space group of Fd-3m [16]. The structure of $LiMn_2O_4$ was showed in Fig. 2A, where Li, Mn and O atoms respectively locate at 8a, 16d and 32e sites. The exchange of positions between Mn and Li atoms in the $LiMn_2O_4$ lattice was confirmed by several groups. Bjork et al. reported that 9% of the lithium ions at the tetrahedral 8a sites can be substituted by Mn^{2+} ions [17]. Martinez et

al. found about 10% of the lithium ions presented at the octahedral 16d sites [18]. Because of the low X-ray scattering factor of Li, the content of Li at Mn positions was ignored in the refinement process. To keep things simple, the existence Ni in the crystal lattice was ignored in the refinement model. In addition, the oxidation number of Mn at 8a sites was set at +2 for all samples.
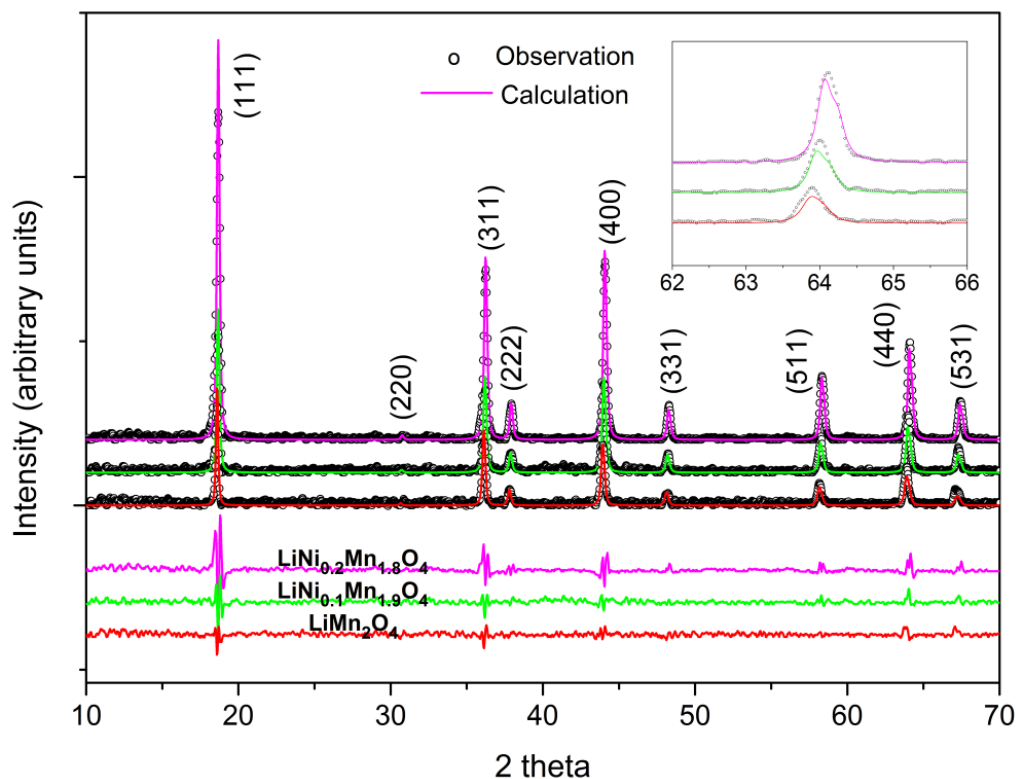

Fig. 3. X-ray powder diffraction patterns and refinement results of LiNi$_x$Mn$_{2-x}$O$_4$ ($x =$ $0, 0.1, 0.2$) materials. The inset shows (440) peak at high magnification.

Figure 3 showed the X-ray diffraction patterns of LiNi$_x$Mn$_{2-x}$O$_4$ samples. All samples were single phase with cubic-spinel structure. It is clear that the X-ray diffraction intensity of the materials increased with the Ni content. This result pointed out the improvement in the crystallinity degree of the materials by substitution effect. Rietveld refinement results of XRD patterns were showed in Table 1. The calculated model was in a good agreement with the experimental results. The doping resulted in the decrease of the lattice constant from 8.2321 Å (LiMn$_2$O$_4$) to 8.2137 Å (LiMn$_{1.8}$Ni$_{0.2}$O$_4$). These results were similar with the reported data [16, 19]. In contrast to the increase of Li–O bond length, Mn–O distance was confirmed to decrease with increasing x-value. Due to the average Mn–O bond length of the Mn^{3+} ion is larger than that of the Mn^{4+} ion [4], the decrease in Mn–O distance can be attributed to the suppression of Jahn–Teller distortion. The substitution of Ni also resulted in the decrease of the content of transition metal at 8a sites, which represents for the structural disorder of LiMn$_2$O$_4$ crystal. The interesting thing here is that although 8a tetrahedral volume increased by ca. 15%, the content of Mn^{2+} ion at 8a

site decreased from 10% to 2% with increasing Ni substitution content. The diffusion of Li^+ ion via 16c octahedral sites was confirmed by many authors [20, 21]. The diffusion mechanism was clarified in Fig. 2B. As it can be seen from Table 1, volume of 16c octahedron was confirmed to increase with decreasing Ni content. The increase of both 8a tetrahedral and 16c octahedral volumes favored for the diffusion of Li^+ ions.

Table 1. Rietveld refinement results of $LiNi_xMn_{2-x}O_4$ ($x = 0, 0.1, 0.2$) materials.

	$LiMn_2O_4$	$LiNi_{0.1}Mn_{1.9}O_4$	$LiNi_{0.2}Mn_{1.8}O_4$
a (Å)	8.2321	8.2228	8.2137
x (O position)	0.2571	0.2614	0.2638
Li–O bond length (Å)	1.8850	1.9458	1.9755
Mn–O bond length (Å)	2.0003	1.9672	1.9467
8a tetrahedral volume ($Å^3$)	3.4375	3.7778	3.9523
16c octahedral volume ($Å^3$)	12.6202	13.2014	13.4483
Mn^{2+} content at 8a site	0.10	0.07	0.02
GOF (Goodness of fit)	1.968	1.664	1.529

The effect of Ni content on the electrical conductivity of the materials was examined by the electrochemical impedance analysis. In this work, the cylindrical pellets can be treated as blocking electrodes where Li^+ ions cannot move in and out of the electrodes. The equivalent circuit of the electrodes is shown in the inset in Fig. 4 where the electrode/current collector contact, the grain boundaries and the bulk material are respectively modeled by $R_1//C_1$, $R_2//CPE_2$ and $R_3//CPE_3$ circuits. The impedance of a constant phase element (CPE) can be expressed as following equation [24]:

$$Z_{CPE} = \frac{1}{T(iw)^p} \tag{1}$$

Here, w and T respectively represent for the angular frequency and the numerical value of the admittance of the CPE. The exponent factor P indicates capacitor behavior of the CPE. The value of P is in the range of 0–1. When P equals to 1, Eq. (1) is identical to the impedance of a capacitor.

The electrochemical impedance spectra of the electrodes have shown in Fig. 4. The fitting results of the electrochemical impedance spectra have been shown in Table 2. It is clear that the increase of Ni content resulted in the increase of R_2 and R_3 value, which respectively represented for the grain boundary and the bulk resistivities of the materials. This result is consistent with the observation of J. Molenda et al. who confirmed the decrease of the conductivity by doping effect [12]. At present, there were experimental and theoretical confirmations that $LiMn_2O_4$ is a mixed ionic-electronic conductor with dominating electronic conduction, and the electronic conduction of the material was closely related to the structural stability of the material [12, 22].
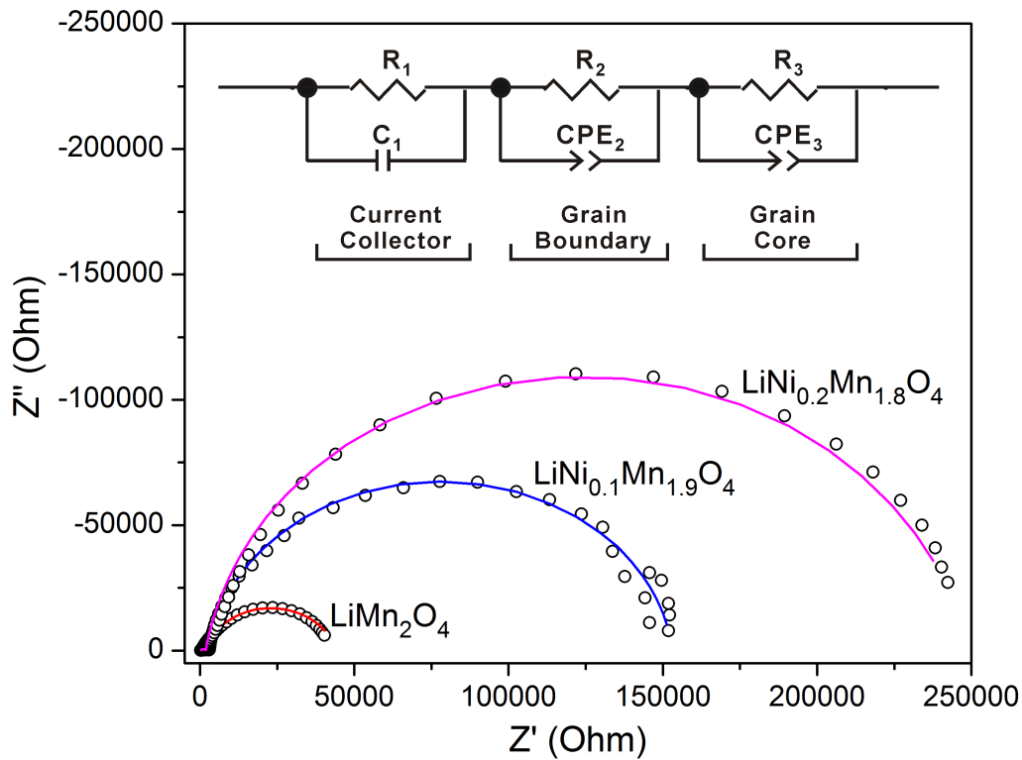
Fig. 4. Nyquist plots of $LiNi_xMn_{2-x}O_4$ (x= 0, 0.1, 0.2) samples. The inset shows the equivalent circuit using for the fitting process.

Table 2. The fitting results of electrochemical impedance data.

	R_1	R_2	R_3	T_3	P_3
$LiMn_2O_4$	101.7	2326.8	41399	8.01E-6	0.8706
$LiNi_{0.1}Mn_{1.9}O_4$	510.0	2498.1	150157	4.22E-7	0.9312
$LiNi_{0.2}Mn_{1.8}O_4$	282.8	2652.1	242857	1.23E-6	0.9323

Generally, the electronic conductivity of a semiconductor will be increased along with the increase of the defect concentration. In other words, the decrease in structural disorder of a semiconductor will result in the decrease of the electronic conductivity of the material. Based on these discussions, it can conclude that the substitution of Ni decreased structural disorder of $LiMn_2O_4$ crystal and resulted in the decrease in the electronic conductivity of the material. In the case of the CPE, which shows the capacitance behavior of the materials, the substitution resulted in the increase of the exponent factor P. It is well known that the exponent factor of a CPE depends on the shape and the morphology of the electrode. In this work, these influences can be eliminated due to the similarity in shape of electrodes and the morphology of the samples. Several groups confirmed

the effect of the heterogeneity of material on the exponent factor of the CPE [25–27]. Based on the data presented herein, it is clear that the substitution of Ni resulted in the improvement of the heterogeneity of the cathode material, which revealed by the increase of the exponent factors of the bulk CPE.

In another approach, the improvement in the conductivity of $LiNi_xMn_{2-x}O_4$ with increasing Ni content was reported by several groups. R. Holze et al. showed that the substitution of Ni in the range of x=0–0.1 caused the increase in the conductivity of $LiNi_xMn_{2-x}O_4$ cathode [23]. The same results are also reported by M. A. Kebede et al. in the range of x=0–0.2 [13]. These results seem to contradict with the impedance results in this work. However, it should be noted that the present authors performed the experiments on a half cell configuration where the conductivity of the cathode limited by Li^+ ionic conductivity and affected by other elements including conducting agent and binder in the cathode. As discussed above, the substitution of Ni not only improved the structural stability of $LiNi_xMn_{2-x}O_4$ but also resulted in the extension of 8a tetrahedron and 16c octahedron which supported for the Li^+ diffusion. Of course, this substitution will result in the improvement of Li^+ ionic conductivity and electrochemical performance of $LiNi_xMn_{2-x}O_4$ cathode materials.

IV. CONCLUSIONS

The effect of Ni substitution on the structure and the ac conduction of $LiNi_xMn_{2-x}O_4$ ($x = 0, 0.1, 0.2$) was investigated. The Rietveld refinement results showed that the substitution decreased Jahn–Teller distortion and improve the structural stability of the materials. As a result, these effects caused the decrease of the electronic and total conductivities of the materials. In contrast, the substitution increased Li^+ conductivity and electrochemical performance of $LiNi_xMn_{2-x}O_4$ which arise from the extension of 8a tetrahedron and 16c octahedron. Due to the electrochemical performance of $LiNi_xMn_{2-x}O_4$ depends on both electronic and ionic conductions, the results from this work suggested the improvement of electronic conduction as a solution for the design of high performance $LiNi_xMn_{2-x}O_4$ cathode materials.

ACKNOWLEDGEMENTS

REFERENCES

[1] T. Ohzuku, M. Kitagawa and T. Hirai, *J. Electrochem. Soc.* **137** (1990) 769–775.
[2] R. Gummow, A. De Kock and M. Thackeray, *Solid State Ionics* **69** (1994) 59–67.
[3] D.H. Jang, Y.J. Shin and S.M. Oh, *J. Electrochem. Soc.* **143** (1996) 2204–2211.
[4] C.Y. Ouyang, S.Q. Shi and M.S. Lei, *J. Alloys Compd.* **474** (1–2) (2009) 370–374.
[5] Y. Xia, T. Sakai, T. Fujieda, X. Yang, X. Sun, Z. Ma, et al., *J. Electrochem. Soc.* **148** (2001) A723–A729.
[6] M. D. Bhatt and C. O'Dwyer, *Phys. Chem. Chem. Phys.* **17** (2015) 4799-4844.
[7] K. Amine, H. Tukamoto, H. Yasuda and Y. Fujita, *J. Power Sources* **68** (1997) 604–608.
[8] R. Alcantara, M. Jaraba, P. Lavela and J. Tirado, *Electrochim. Acta* **47** (2002) 1829–1835.
[9] M. M. Thackeray, A. de Kock, M. H. Rossouw, D. C. Liles, R. Bittihn and D. Hoge, *J. Electrochem. Soc.* **139** (1992) 363.
[10] F. Le Cras, P. Strobel, M. Anne, D. Bloch, J. P. Soupart and J. C. Rousche, Eur. *J. Solid State Inorg. Chem.* **33** (1996) 67.

[11] H. Berg, K. Goransson, B. Nolang and J. O. Thomas, *J. Mater. Chem.* **10** (2000) 1437-1441.

[12] J. Molenda, J. Marzec, K. Swierczek, W. Ojczyk, M. Ziemnicki, M. Molenda, M. Drozdek, R. Dziembaj, *Solid State Ionics* **171** (3–4) (2004) 215–227.

[13] M. A. Kebede, N. Kunjuzwa, C. J. Jafta, M. K. Mathe, K. I. Ozoemena, *Electrochim. Acta* **128** (2014) 172–177.

[14] J. Rodríguez-Carvajal, *FullProf Program: Rietveld, Profile Matching and Integrated Intensities Refinement of x-Ray and/or Neutron Data (Powder and/or Single-Crystal)*. Laboratoire Leon Brillouin (CEA-CNRS), 2007.

[15] K. Momma and F. Izumi, *J. Appl. Cryst.* **41** (2008) 653-658.

[16] Q. Zhong, A. Bonakdarpour, M. Zhang, Y. Gao and J. R. Dahn, *J. Electrochem. Soc.* **144** (1) (1997) 205-213.

[17] H. Bjork, H. Dabkowska, J. E. Greedan, T. Gustafsson, J. O. Thomas, *Acta Crystallogr., Sect. C: Cryst. Struct. Commun.* **57** (2001) 331–332.

[18] S. Martinez, I. Sobrados, D. Tonti, J. M. Amarilla and J. Sanz, *Phys. Chem. Chem. Phys.* **16** (2014) 3282–3291.

[19] Y. Wei, K. B. Kim, G. Chen, *Electrochim. Acta* **51** (16) (2006) 3365–3373.

[20] M.M. Thackeray, W.I.F. David, P.G. Bruce, J.B. Goodenough, *Mater. Res. Bull.* **18** (4) 1983 461-472.

[21] N. Ishizawa, K. Tateishi, *J. Ceram. Soc. Jpn.* **117** (2009) 6-14.

[22] K. Hoang, *J. Mater. Chem. A* **2** (2014) 18271-18280.

[23] F.X. Wang, S.Y. Xiao, Y. Shia, L.L. Liu, Y.S. Zhu, Y.P. Wu, J.Z. Wang, R. Holze, *Electrochim. Acta* **93** (2013) 301–306.

[24] Scully J.R., Silverman D.C., Kendig M.W., *Electrochemical impedance: analysis and interpretation*. American Society for Testing and Materials, Philadelphia 1993.

[25] C.-H. Kim, S.-I. Pyun and J.H. Kim, *Electrochim. Acta* **48** (2003) 345.

[26] Z. Kerner and T. Pajkossy, *J. Electroanal. Chem.* **448** (1998) 139.

[27] J.-B. Jorcin, M. E. Orazem, N. Pébère, and B. Tribollet, *Electrochim. Acta* **51** (2006) 1473.